American Mineralogist, Volume 65, pages 8–25, 1980

Mineralogy and petrology of very-low-metamorphic grade Archaean banded iron-formations, Weld Range, Western Australia

MARTIN J. GOLE[1]

Department of Geology, University of Western Australia
Nedlands 6009, Australia

Abstract

There are two basic Fe-rich lithologies at Weld Range: (1) banded iron-formation containing minnesotaite, siderite, quartz, magnetite, greenalite, stilpnomelane, pyrite, and chamosite with trace amounts of pyrrhotite, arsenopyrite, chalcopyrite, apatite, and rockbridgeite; (2) Fe-shale, which occurs as laminated 2–30cm-thick bands within banded iron-formation, containing chamosite, stilpnomelane, siderite, greenalite, pyrite, magnetite, minnesotaite, and quartz with trace amounts of ilmenite, chalcopyrite, and apatite. Mineral assemblages, mineral compositions, and the interpreted paragenetic sequence in both lithologies are essentially the same as those reported from very-low-metamorphic grade Proterozoic iron-formations. In common with published greenalite analyses, those of greenalite from the Weld Range show a consistent excess of Si and a larger than corresponding deficiency in octahedral sites relative to the generally accepted formula of $(Fe,Mg)_6Si_4O_{10}(OH)_8$. The earliest recognizable mineral assemblages contain Al-bearing greenalite (1.9–2.8 wt% Al_2O_3), quartz, siderite, chamosite, magnetite, pyrite, and rarely pyrrhotite. These assemblages are overprinted by stilpnomelane, which formed by reaction of a K-bearing fluid phase with Al-bearing greenalite or chamosite or both. A secondary Al- and Mg-poor greenalite developed in some assemblages contemporaneously with stilpnomelane. The presence of quartz favored the growth of coarse-grained stilpnomelane. The relatively coarse grain size of quartz and siderite (up to 2.5mm) and the presence of angular fragments composed of early assemblages in intraformational breccia indicates that the Fe-rich lithologies were well lithified prior to the development of stilpnomelane. The incoming of minnesotaite occurred after that of stilpnomelane, and textures indicating reaction of earlier silicates and siderite to form minnesotaite are common. The assemblage minnesotaite–quartz±magnetite±pyrite represents the complete reaction of the earlier assemblages. The early assemblages are preserved in bulk compositions which are Si-deficient or Al-rich or both, and under conditions of relatively low P_{O_2} or high P_{CO_2} or both. The peak metamorphic temperature is estimated to be 320±50°C at low pressure.

Introduction

Banded iron-formation is a widely distributed although relatively minor (<1–3 vol%) lithology in the stratigraphic successions of the 2.6–2.7 Gyr greenstone belts of the Yilgarn Block, Western Australia. The Weld Range (Fig. 1) is one of the few localities in the Yilgarn Block from which samples of unweathered, very-low-metamorphic grade banded iron-formation are available. In the eastern half of the Yilgarn Block, the metamorphic grade in greenstone belts ranges from prehnite–pumpellyite to upper amphibolite facies (Binns *et al.*, 1976, p. 303–313), and similar variations in metamorphic grade occur in the greenstone belts in the northwest of the block. The mineralogy of banded iron-formations together with that of juxtaposed tholeiitic metabasalts and less commonly of pelitic metasediments indicates that most of the banded iron-formations in the greenstone belts have been metamorphosed to grades between those of the upper greenschist and the upper amphibolite facies. Banded iron-formation of lower metamorphic grade is relatively uncommon, and few such banded iron-formations have been diamond-drilled to depths below the zone of weathering.

The Weld Range is a marked physiographic feature, 3–5km wide, 40km long, within which there is

[1] Present address: Department of Geology, Indiana University, Bloomington, Indiana 47405.

0003–004X/80/0102–0008$02.00

good exposure of metabasites showing mainly doleritic and minor basaltic and gabbroic textures. Such exposures occur between ridges defined by weathered, steeply dipping beds of banded iron-formation which form less than 10% of the thickness of the sequence. Poorly exposed, very fine-grained clastic metasediments form a very minor part of the sequence. In the Mt. Lulworth area, in the central part of the Weld Range, variations in the mineralogy of metabasites indicate a gradient in metamorphic conditions from the lowermost greenschist facies in the north to approximately the greenschist–amphibolite facies transition in the south.

Core samples of banded iron-formation were selected from diamond-drill hole No. 3 (D.D.H. 3), drilled by the Western Australia Department of Mines during iron ore exploration in the early 1960's (Jones, 1963). D.D.H. 3 is located on the northern side of the Weld Range, 2km northeast of Mt. Lulworth (Fig. 1), and was drilled below a prominent ridge of highly weathered banded iron-formation. The hole intersected two beds of banded iron-formation within a sequence of very fine-grained quartz–chlorite-rich metasediments. The broad distribution of rock types in D.D.H. 3 and sample locations are given in Figure 2. Most samples show some evidence of secondary oxidation due to weathering, and parts of the banded iron-formation, even in the deepest sections of the hole, are highly altered. In essentially unweathered sections of core, the banded iron-formation contains well-preserved, arrested reaction textures showing a texturally early mineral assemblage overprinted by several generations of later minerals. The minerals in the banded iron-formation, in approximate decreasing order of abundance, are minnesotaite, siderite, quartz, magnetite, greenalite, stilpnomelane, pyrite, and chamosite. Trace amounts of pyrrhotite, arsenopyrite, chalcopyrite, and apatite are widely distributed, and rockbridgeite, first reported by Jones (1963), occurs in trace amounts in two samples. Mineral proportions, however, vary widely and over large sections of the core some of the minerals listed above are absent (Fig. 2). Much of the banded iron-formation is mesobanded, and very different mineral assemblages commonly

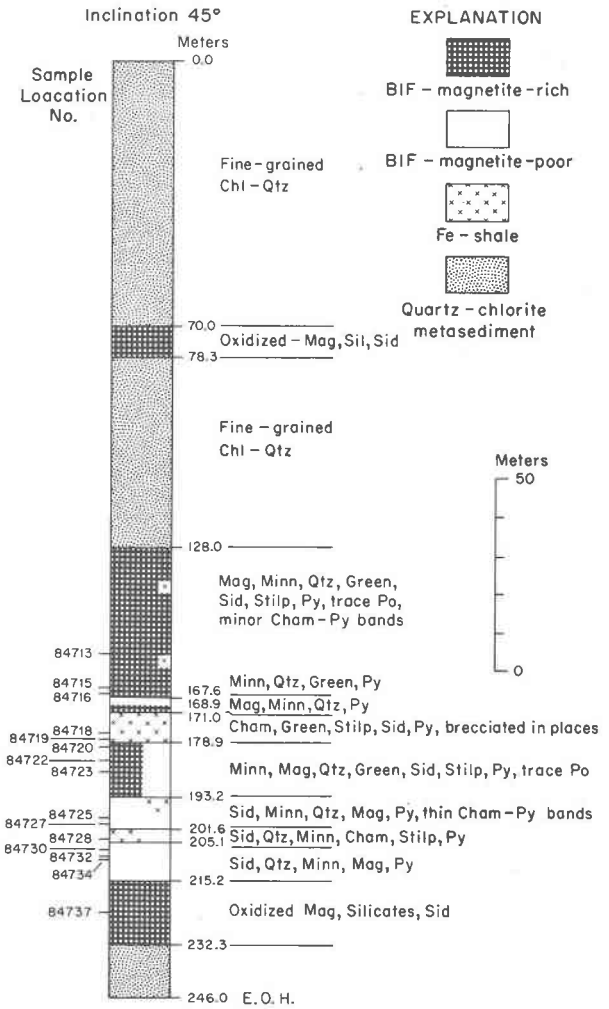

Fig. 2. Graphic log of D.D.H. 3, Weld Range. Minerals are listed in order of approximate decreasing relative abundance. Most contacts shown are gradational. Direction of the stratigraphic top is not known. Estimated thickness of the main banded iron-formation is 70–90m.

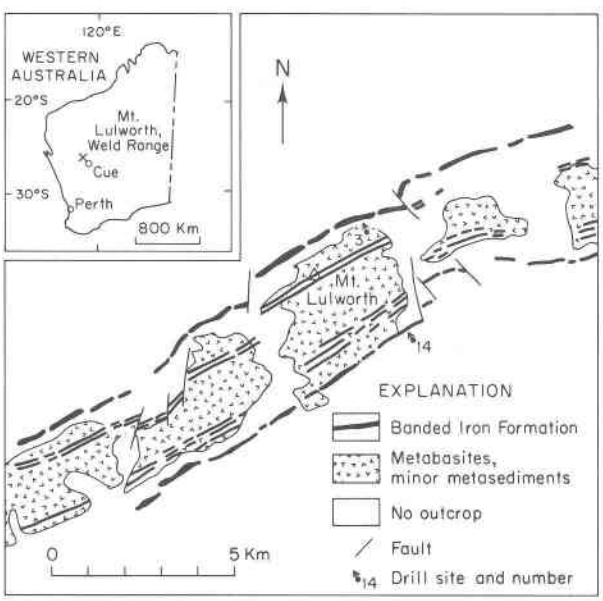

Fig. 1. Location and geological sketch map of the central part of the Weld Range, Western Australia (after Jones, 1963).

occur in adjacent mesobands. Within the banded iron-formation, 2–30cm-thick bands of massive to laminated Fe-rich shales occur, having both mineralogically sharp and gradational contacts with the banded iron-formation. The minerals in the Fe-shale, in approximate decreasing order of abundance, are chamosite, stilpnomelane, siderite, greenalite, pyrite, magnetite, minnesotaite, and quartz. Trace amounts of ilmenite, chalcopyrite, and apatite are also present.

This study is the first detailed description of the mineralogy and petrology of very-low-metamorphic grade banded iron-formation of the Archaean. It will be shown that the mineral assemblages, the mineral compositions, and many of the textural relations in the banded iron-formation at Weld Range are essentially identical to those of the well-studied major Proterozoic iron-formations.

Table 1. Chemical analyses of bulk samples of banded iron-formation and Fe-shale from D.D.H. 3, Weld Range

		1	2	3	4
	SiO_2	49.76	14.52	21.20	27.05
	TiO_2	0.01	0.12	0.00	0.27
	Al_2O_3	0.26	0.54	0.08	6.26
	Fe_2O_3	17.45	1.83	16.15	17.09
	FeO	24.65	44.92	34.82	25.26
	MnO	0.17	1.86	1.43	0.92
	MgO	2.50	2.13	7.97	5.47
	CaO	0.31	0.55	0.69	0.09
	Na_2O	0.03	0.02	0.04	0.03
	K_2O	0.02	0.20	0.01	0.33
	H_2O^+	2.47	0.07	1.95	6.00
	H_2O^-	0.12	0.06	0.17	0.95
	P_2O_5	0.22	0.20	0.37	0.03
	CO_2	0.40	32.05	15.50	7.57
	S	1.00	0.72	0.03	4.33
		99.37	99.79	100.41	101.65
	-O = S	0.25	0.18	0.01	1.08
		99.12	99.61	100.40	100.57
	Fe^{3+}	12.20	1.28	11.30	11.95
Fe^{2+}	Sulfide	0.86	0.63	0.03	3.76
	Other	18.30	34.29	27.04	15.87
	Total Fe	31.36	36.20	38.27	31.58
	Fe^{3+}/Fe^{2+}	0.67	0.04	0.42	0.75

1. BIF consisting of minn, qtz, mag, sid, stilp, green, py. Sample 84723. Depth 186.2-186.5m; 2. BIF consisting of sid, qtz, mag, minn, stilp, green, py. Sample 84725. Depth 198.1-198.4; 3. BIF consisting of minn, sid, qtz, mag, stilp. Sample 84730. Depth 206.0-206.4m; 4. Fe-shale consisting of cham, stilp, sid, qtz, mag, py, minn. Sample 84728. Depth 203.0-203.1m.

Analytical methods

Bulk chemical analyses were obtained by XRF except for Na_2O (AAS), FeO (titration against potassium dichromate), H_2O and CO_2 (gravimetry), and S (Leco furnace). Electron microprobe analyses were performed using an automated, 3-spectrometer ARL-SEMQ electron probe microanalyzer. For silicates and carbonates, a series of natural minerals were used for primary and secondary standards and the data reduced by the method of Bence and Albee (1968), using the alpha factors of A. A. Chodos (unpublished). Estimates of H_2O for silicates and CO_2 for carbonates were made for purposes of the reduction procedure. Sulphide probe analyses were performed using pyrite and gallium arsenide as standards and Magic IV (Colby, 1971) for data reduction.

Electron microprobe analyses with the same sample number refer to a single mesoband within the sample. Samples are housed in the Rock Store of the Department of Geology, University of Western Australia.

Bulk chemical analyses

Bulk chemical analyses of banded iron-formation and Fe-shale (Table 1, anal. 1 to 3, and 4, respectively) illustrate three features that reflect important aspects of their mineralogy. (a) The CaO content, even of the most CO_2-rich sample, is negligible, which indicates that the carbonate is siderite. (b) The relatively low Fe^{3+}/Fe^{2+} ratios reflect the presence of abundant siderite and Fe^{2+}-silicates and the generally low proportion of magnetite. No hematite was identified as part of the unaltered, low-metamorphic grade assemblages, and all hematite appears to be due to weathering. (c) Both the banded iron-formation and the Fe-shale bands are relatively S-rich.

Mineral chemistry

The minerals that are part of the paragenetically early assemblages in the banded iron-formation from D.D.H. 3 are greenalite, chamosite, siderite, quartz, magnetite, sulfides, and apatite. Stilpnomelane, minnesotaite, and perhaps rockbridgeite, which occurs in veinlets, are paragenetically late. The chemistry of these minerals will be discussed in the above order in the following sections with the exception of apatite and rockbridgeite, which will not be discussed further.

Greenalite

In accordance with the work of Gruner (1936), 1946), it has generally been assumed that greenalite

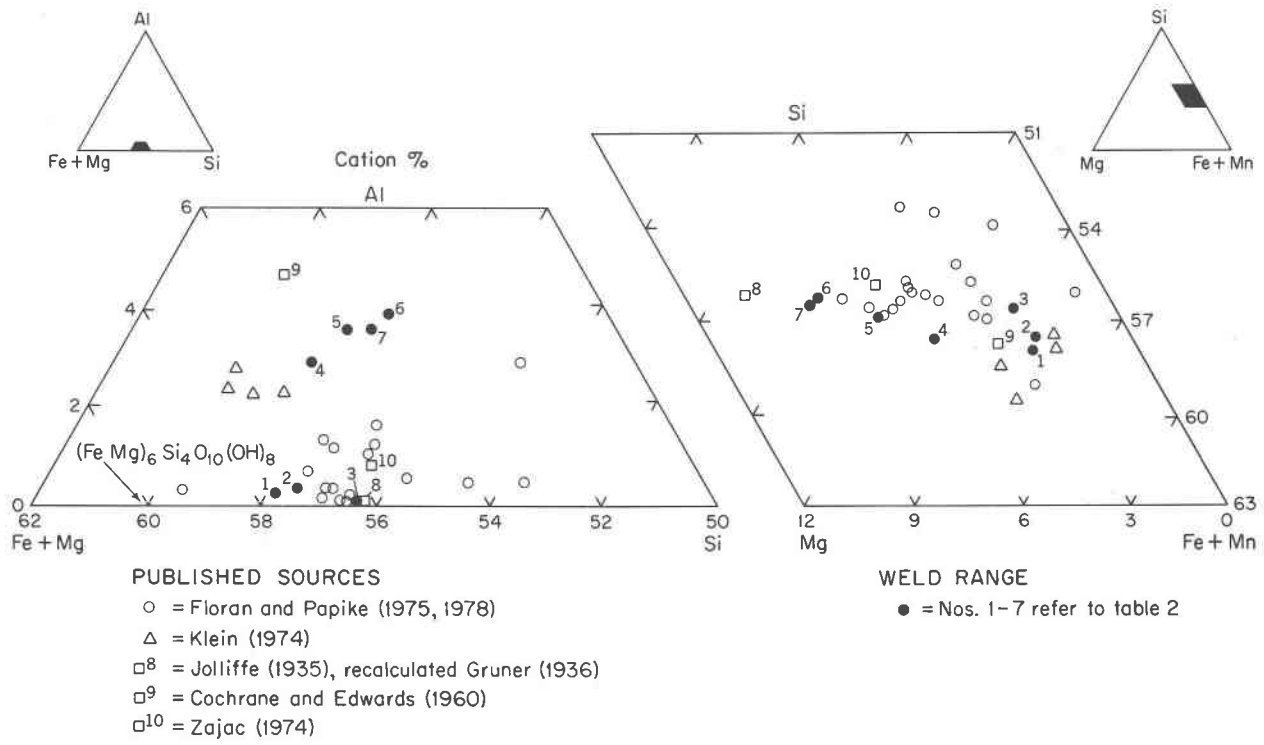

Fig. 3. Compositional variations in greenalite plotted within the systems (Fe+Mn)–Mg–Si and (Fe+Mg)–Al–Si.

has an idealized formula of $Fe_6Si_4O_{10}(OH)_8$, and that it is the structural analogue of antigorite. The generally very fine-grained intergrowths of greenalite with other minerals make compositions determined on mineral separates rather unreliable, and the fine grain size of greenalite (Klein, 1974; Floran and Papike, 1975; this study) has made single-crystal structural determinations difficult. However, there are now a sufficient number of reliable electron microprobe analyses which, together with the first single-crystal structural data, suggest that the crystal chemistry of greenalite is more complicated than previously considered.

It has only recently become clear from electron microprobe analyses (Klein, 1974; Floran and Papike, 1975, 1978; Table 2; see Fig. 3) that most analyses of greenalite, when recalculated on an anhydrous basis of 14 oxygens, show an excess of Si over that required to fill the assumed tetrahedral site occupancy of 4.00. These analyses also show a larger than corresponding deficiency in the octahedral site. Several reasons for these features have been proposed. Klein suggested the presence of submicroscopic intergrowths of chert in greenalite as the cause of the excess Si, and Floran and Papike (1975) interpreted their greenalite analyses as being the result of a mixed layer phase composed of the end-members greenalite and minnesotaite. The recent X-ray and electron diffraction study of greenalite by Guggenheim *et al.* (1977), using for the first time a single crystal of greenalite, has suggested a structural reason for the deviation of the greenalite composition from the ideal formula. They suggest (S. W. Bailey, personal communication, 1977) that greenalite consists of a coherent intergrowth of a dominant trigonal layer-silicate phase with a second, minor, structurally inverted monoclinic phase. They reason that the inversion has caused a loss of Mg and OH where the phases interfere, giving an apparent excess Si content. In this respect it is similar to antigorite which also has excess Si (Page, 1968; Whittaker and Wicks, 1970), but there is no evidence for a wave-like superstructure in greenalite (S. W. Bailey, personal communication, 1977).

In published analyses and my electron microprobe analyses of greenalite, Al_2O_3 ranges from trace amounts to a little over 3.0 wt% (Fig. 3). Coexistence of greenalite and chamosite in the banded iron-formation from D.D.H. 3 suggests that the Al_2O_3 value of 3.0 wt% is probably close to a maximum. Al-rich greenalites have lower Si contents than Al-poor greenalites (Table 2), which suggests that some Al

Table 2. Representative electron microprobe analyses of greenalite from D.D.H. 3, Weld Range

	1	2	3	4	5	6	7
SiO_2	33.9	34.2	34.9	34.1	34.5	35.5	35.2
TiO_2	0.01	0.01	0.01	0.03	0.03	0.04	0.02
Al_2O_3	0.12	0.22	0.02	1.90	2.43	2.76	2.45
FeO[1]	52.8	52.2	50.9	49.3	47.3	46.0	45.8
MnO	0.34	0.34	0.50	0.50	0.50	0.48	0.47
MgO	1.67	1.53	1.57	3.07	3.76	4.59	4.65
CaO	0.02	0.03	0.01	0.02	0.02	0.00	0.02
Na_2O	0.01	0.04	0.02	0.04	0.01	0.00	0.01
K_2O	0.01	0.02	0.01	0.02	0.01	0.00	0.01
Total	88.88	88.59	87.94	88.98	88.56	89.37	88.63
	Ions on the basis of 14 oxygens						
Si	4.13	4.16	4.24	4.05	4.06	4.09	4.09
Al	0.02	0.03	0.00	0.27	0.34	0.37	0.34
Fe	5.37	5.31	5.18	4.90	4.66	4.43	4.45
Mn	0.03	0.04	0.05	0.05	0.05	0.05	0.05
Mg	0.30	0.28	0.29	0.54	0.66	0.79	0.81
Ca	0.00	0.00	0.00	0.00	0.00	0.00	0.00
Na	0.00	0.01	0.01	0.01	0.00	0.00	0.00
ΣOCT	5.72	5.67	5.53	5.77	5.71	5.64	5.65

[1] *All Fe as FeO*

1. Slightly brown green in intergrowth with stilp, sid and qtz. N = 4. Sample 84715/2; 2. Slightly brown green with minor dark diffuse patches (<1 μm) intergrown with sid and qtz. N = 5. Sample 84715/1; 3. Pleochroic green to pale brown, fibrous green rim on sid-py-po nodule in minn-qtz-rich mesoband. N = 4. Sample 84734; 4. Clear green in similar intergrowth as 2 above. N = 6. Sample 84715/1; 5. Green from green-sid-py-stilp mesoband. N = 7. Sample 84716; 6 and 7. Green from mesoband containing green, sid minn, stilp, cham, py. Sample 84718.

substitutes for Si despite the apparent excess of the latter.

Because Fe^{3+} cannot be determined directly by the electron microprobe, all Fe has been assumed to be FeO in microprobe analyses. In published wet-chemical analyses the amount of Fe_2O_3 has been assumed to be due to secondary oxidation of FeO (*e.g.* Floran and Papike, 1975). The assumption of all Fe as FeO in greenalite is probably a good first approximation. In one retrograde assemblage in a highly metamorphosed banded iron-formation from the Yilgarn Block, greenalite coexists with a mineral which is probably related to cronstedtite, an Fe^{3+}-bearing 7A phyllosilicate (Gole, in preparation). This occurrence suggests that greenalite is mainly a Fe^{2+} mineral and that available Fe^{3+} is preferentially housed in other minerals, either silicates or oxides.

As noted by Klein (1974) and Floran and Papike (1975), there is a relatively narrow range in MgO content in greenalite from low-grade iron-formations (Fig. 3).

The greenalites from the Weld Range have chemical compositions that are broadly similar to previously published analyses (Fig. 3). However, they have, on average, lower Si contents than greenalites from the Gunflint Iron Formation (see Floran and Papike, 1975, 1978).

In the Weld Range banded iron-formation, two distinct greenalite compositions occur. Greenalites which are Al-rich (1.90–2.76 wt% Al_2O_3) have moderate MgO contents (3.07–4.65 wt%) whereas greenalites that are Al-poor (0.02–0.22 wt% Al_2O_3) have relatively low MgO contents (1.53–1.67 wt%) (Table 2, Fig. 3). The different compositions correspond to different textures in which the greenalite occurs (discussed below). The Fe/(Fe+Mg) ratio of the Al-rich greenalite varies slightly between mesobands (Fig. 3), and within any one mesoband this ratio does not appear to be affected by assemblages. Greenalite consistently has the highest Fe/(Fe+Mg) ratio of any of the Fe-silicates or carbonates in a given mesoband (Fig. 4).

Some greenalite contains submicroscopic dark diffuse patches. In places, the patches are so dense that the greenalite is opaque in plane light. Electron probe analyses show no distinctive chemical differences between greenalite containing patches and

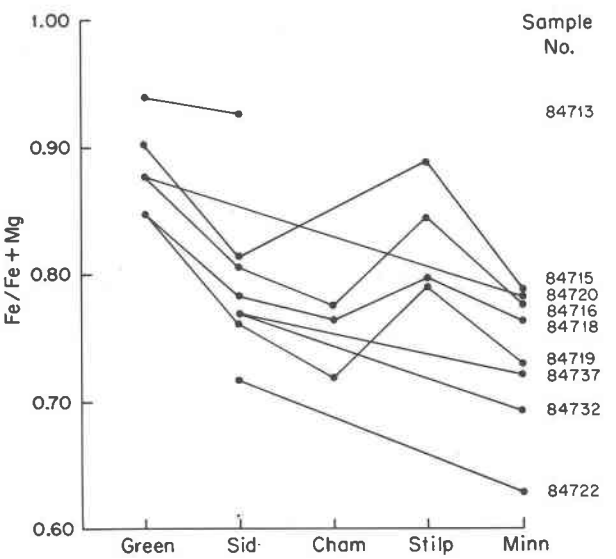

Fig. 4. Fe/(Fe+Mg) ratios of electron microprobe analyses of minerals from D.D.H. 3 Weld Range. Tielines join minerals from the same mesoband. Greenalites plotted are Al-bearing.

clear greenalite. It is unknown whether these patches are inclusions in or an alteration of greenalite. Zajac (1974, p. 116) reported similar features in greenalite from the Sokoman Iron Formation.

Chamosite

Most chamosites in this study show small 14A peaks, indicating that they are probably mixed-layer silicates. Chamosites in Fe-shale have larger 14A peaks relative to their 7A peaks than chamosites from banded iron-formation. When recalculated on a basis of 14 oxygens, chamosites in Table 3 have excess octahedral cations. Recalculation of the analyses on a fixed-cation basis suggests that small amounts of Fe^{3+} may be present. The presence of Fe^{3+} is also consistent with the balancing of tetrahedral Al with octahedral Al + Fe^{3+} in most analyses. Even assuming considerable Fe^{3+} is present, the octahedral site in Weld Range chamosites is filled to a greater extent than in more recent chamosites (Weaver and Pollard, 1973). This may be because the Weld Range chamosites are mixed-layer 7–14A phyllosilicates.

Where chamosite occurs as a minor constituent in banded iron-formation it is very Fe-rich. The most Mg-rich chamosites are found in the Fe-shale bands (Table 3), indicating that their Fe/(Fe + Mg) ratio is largely controlled by bulk chemistry. Chamosites have low Fe/(Fe + Mg) ratios relative to coexisting Fe-silicates and carbonates (Fig. 4).

Carbonates

Siderite is the only carbonate found in the banded iron-formation of D.D.H. 3. It shows a narrow range in Fe/(Fe + Mg) ratios within a single mesoband but a considerable spread between mesobands (Table 4). Siderites with the highest MgO content occur in a mesoband with the unusual assemblage of siderite–minnesotaite–chamosite–pyrite–pyrrhotite (Table 4, anal. 3). However, in the adjacent mesoband siderite is relatively Fe-rich (Table 4, anal. 4). The CaO content of siderite is generally low (0.04–1.92 wt%), and the MnO content ranges from 0.05 to 5.65 wt%. Secondary siderite, occurring in a vein within quartz, has a marginally different composition from primary siderite in the same mesoband (Table 4, anal. 6 and 7).

Quartz, magnetite, and sulfides

In the banded iron-formation and Fe-shale from D.D.H. 3, quartz grain sizes are easily observed under high magnification and range from 0.3 to 2.0mm across with rare grains up to 2.5mm.

In iron-formations, magnetite generally has a pure end-member composition (*e.g.* Klein, 1974). Electron microprobe analyses of magnetite and ilmenite in Fe-shale assemblages show them also to have near end-member compositions. The compositions of pyrrhotite and arsenopyrite coexisting with pyrite are given in Table 5. Pyrrhotite and arsenopyrite from samples where they are not in contact with each other or do not coexist with pyrite have similar compositions to those in Table 5.

Stilpnomelane

Electron microprobe analyses of stilpnomelane from D.D.H. 3 (Table 6) have been recalculated on a

Table 3. Representative electron microprobe analyses of chamosite from D.D.H. 3, Weld Range

	1	2	3	4
SiO_2	22.9	23.3	24.0	23.6
TiO_2	0.00	0.06	0.03	0.04
Al_2O_3	19.4	20.2	18.0	19.0
FeO[1]	37.5	34.9	33.5	30.2
MnO	0.17	0.12	0.11	0.15
MgO	6.48	7.60	10.58	12.15
CaO	0.02	0.18	0.04	0.00
Na_2O	0.04	0.03	0.09	0.01
K_2O	0.00	0.01	0.00	0.00
Total	86.51	86.40	86.35	85.15
	Ions on the basis of 14 oxygens			
Si	2.64	2.64	2.72	2.66
Al	1.36	1.36	1.28	1.34
ΣTET	4.00	4.00	4.00	4.00
Al	1.28	1.35	1.11	1.13
Ti	0.00	0.01	0.00	0.00
Fe	3.62	3.32	3.16	2.85
Mn	0.02	0.01	0.01	0.01
Mg	1.11	1.29	1.78	2.04
Ca	0.00	0.02	0.01	0.00
Na	0.01	0.01	0.02	0.00
ΣOCT	6.04	6.01	6.09	6.03

[1] *All Fe as FeO*

1. Cham coexisting with green, sid and py. Sample 84718; 2. Cham with green and py in breccia fragments cemented by sid. Sample 84719; 3. Cham with stilp, sid, py, minor mag and qtz in Fe-shale band. Sample 84728; 4. Cham with py, stilp and sid in Fe-shale band. Sample 84727.

Table 4. Representative electron microprobe analyses of siderite from D.D.H. 3, Weld Range

	1	2	3	4	5	6	7
FeO[1]	59.7	52.0	46.2	54.0	46.1	45.7	46.3
MnO	0.05	4.10	0.44	3.32	5.35	4.78	5.65
MgO	0.15	2.33	10.13	1.25	5.94	6.20	3.34
CaO	0.04	1.64	0.48	0.78	1.02	0.77	1.92
Total	60.00	60.21	57.39	59.50	58.53	57.57	57.30
	Ions on the basis of 6 oxygens						
Fe	1.88	1.62	1.35	1.68	1.39	1.36	1.39
Mn	0.00	0.13	0.01	0.10	0.16	0.14	0.17
Mg	0.01	0.13	0.53	0.07	0.32	0.33	0.18
Ca	0.00	0.07	0.02	0.03	0.04	0.03	0.07
Total	1.89	1.95	1.91	1.88	1.91	1.86	1.81
C	2.06	2.03	2.04	2.06	2.04	2.07	2.09

[1] *All Fe as FeO.*

1. Sid from sid-sul nodule with Al-poor green vein. Sample 84734; 2. Similar occurrence as 1 above. Sample 84713; 3. Sid from sid-cham-py-po-minn mesoband. Sample 84722; 4. Sid in mag-rich mesoband adjacent to 8 above. Sample 84722; 5. Sid from sid-green-stilp assemblage. Sample 84715/1; 6. Sid from green-sid mesoband. Sample 84716; 7. Secondary sid vein in quartz near minn-qtz-green-sid intergrowth. Sample 84716.

fixed cation basis, assuming a simplified structural formula of $K_{0.6}(Fe,Mg)_6(Si_8Al)(O,OH)_{27}2–4H_2O$ (Eggleton and Chappell, 1978). This formula is an approximation, and the estimated Fe_2O_3 contents of stilpnomelane in Table 6 are, at best, rough estimates. In banded iron-formation and Fe-shale from the D.D.H. 3 locality, all stilpnomelane is brown. Considering the relatively low Fe^{3+}/Fe^{2+} ratios of the bulk chemical analyses (Table 1) and the abundance of Fe^{2+}-rich minerals in contact with stilpnomelane (most commonly, minnesotaite, siderite, greenalite, and chamosite), it is probable that much of the Fe_2O_3 content of stilpnomelane (as reflected by its coloring) is due to secondary oxidation during weathering (see Eggleton, 1972).

Stilpnomelane from low-grade iron-formations shows a relatively wide range in FeO+MnO, MgO, and Al_2O_3 (Fig. 5) and K_2O contents (0.07–3.57 wt%

Table 5. Electron microprobe analyses of arsenopyrite and pyrrhotite coexisting with pyrite from sample 84715/1, D.D.H. 3, Weld Range

	Arsenopyrite 5		Pyrrhotite 4	
wt %		SD		SD
Fe	35.51	(0.30)	60.29	(0.25)
As	42.70	(0.17)		
S	21.49	(0.42)	38.55	(0.36)
	99.70		98.84	
at %				
Fe	33.71		47.31	
As	30.22			
S	36.07		52.69	
	100.00		100.00	

Table 6. Representative electron microprobe analyses of stilpnomelane from D.D.H. 3, Weld Range

	1	2	3	4	5	6
SiO_2	45.8	45.0	44.8	48.8	45.8	44.5
TiO_2	0.00	0.01	0.00	0.02	0.00	0.01
Al_2O_3	4.22	4.73	4.37	4.28	4.08	5.21
FeO[1]	35.7	35.1	32.8	32.6	33.8	31.8
MnO	0.16	0.18	0.13	0.19	0.20	0.11
MgO	2.55	2.55	3.35	4.70	5.06	6.14
CaO	0.14	0.01	0.09	0.16	0.11	0.10
Na_2O	0.62	0.33	0.17	0.16	0.18	0.14
K_2O	1.58	1.85	1.76	1.24	1.14	1.31
Total	90.77	89.76	87.47	92.15	90.37	89.32
Fe_2O_3[2]	38.51	37.62	34.95	33.12	37.56	35.34
FeO	1.05	1.25	1.35	2.80	.00	.00
Total	94.63	93.53	90.97	95.47	94.03	92.86
	Ions on the basis of 15.63 cations					
Si	8.14	8.09	8.22	8.44	8.09	7.94
Al	0.86	0.91	0.78	0.56	0.85	1.06
ΣTET	9.00	9.00	9.00	9.00	8.94	9.00
Al	0.02	0.09	0.17	0.31	0.00	0.04
Fe^{3+}	5.15	5.09	4.83	4.31	5.00	4.75
Fe^{2+}	0.16	0.19	0.21	0.41	0.00	0.00
Mn	0.02	0.03	0.02	0.03	0.03	0.02
Mg	0.68	0.68	0.92	1.21	1.33	1.63
Ca	0.03	0.00	0.02	0.03	0.02	0.02
Na	0.21	0.12	0.06	0.05	0.06	0.05
K	0.36	0.42	0.41	0.27	0.26	0.30
ΣOCT	6.63	6.62	6.63	6.62	6.70	6.81

[1] *All Fe as FeO*

[2] *Fe_2O_3 estimated assuming formula of $K_{0.6}(Fe,Mg)_6(Si_8Al)(O,OH)_{27}$*

1. Coarse-grained stilp (200-400 μm) which cuts across intergrowth of Al-poor green, sid and qtz. Sample 84715/2; 2. Similar textural occurrence as above. Sample 84715/1; 3. Fine-grained stilp (50-100 μm) in Al-bearing greenalite-sid mesoband. Sample 84716; 4. Stilp sheaves in Al-bearing green-cham-py mesoband. Sample 84718; 5. Stilp needles which cut across contact of cham-green-py breccia fragments and sid cement. Sample 84719; 6. Stilp sheaves in matrix of cham in Fe-shale band. Sample 84728.

K_2O). Those from the Weld Range, however, show a relatively small compositional variation (Fig. 5). Within a mesoband, stilpnomelane compositions are similar regardless of the minerals with which they are in contact.

Minnesotaite

Gruner (1944) showed that minnesotaite, $Fe_3Si_4O_{10}(OH)_2$, has a structure similar to that of talc. However, Guggenheim *et al.* (1977) report on the basis of TEM photographs that minnesotaite has a new layer-like structure. Unfortunately, no details are yet available.

It appears that a complete compositional region exists between minnesotaite and talc in low-grade iron-formations (Fig. 6). These minerals display the widest range of Fe/(Fe+Mg) ratios of all the Fe-silicate minerals in low-grade iron-formations. Relative to greenalite, stilpnomelane, and siderite, minnesotaite has a low Fe/(Fe+Mg) ratio, similar to that of chamosite in the same mesoband (Fig. 4). Small but significant amounts of Al_2O_3 and K_2O may be present in minnesotaite (Table 7).

Recalculation of analyses on the basis of 11 oxygens generally shows agreement with the ideal formula, except that the sum of the octahedrally coordinated ions is consistently in excess of 3.00 (Table 7), which suggests that a small Fe^{3+} component may be present.

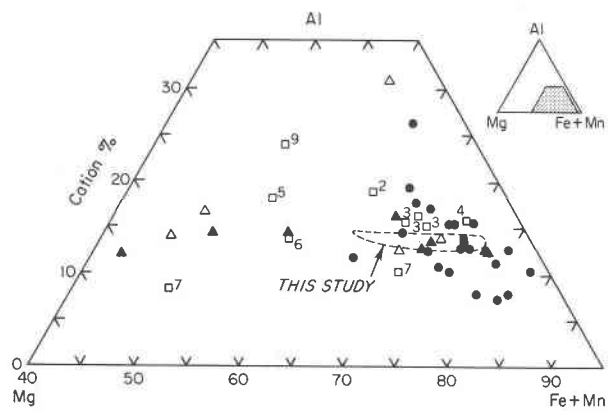

BIWABIK IRON FORMATION
□1 = Grout and Theil (1924)

CRYSTAL FALLS
□2 = Ayres (1940)

CUYUNA IRON FORMATION
□3 = Blake (1965)
□4 = Brown (1971)

BROCKMAN IRON FORMATION
□5 = La Berge (1966a)
□6 = Trendall and Blockley (1970)
□7 = Ayres (1972)
□8 = Miyano (1976)

SOUTH AFRICA
□9 = La Berge (1966 b)

GUNFLINT IRON FORMATION
● = Floran and Papike (1975, 1978)

SOKOMAN IRON FORMATION
▲ = Klein (1974)
▲ = Klein and Fink (1976)
△ = Lesher (1978)

Fig. 5. Compositional variation in stilpnomelane from very-low-metamorphic grade banded iron-formations plotted within the system (Fe+Mn)–Mg–Al.

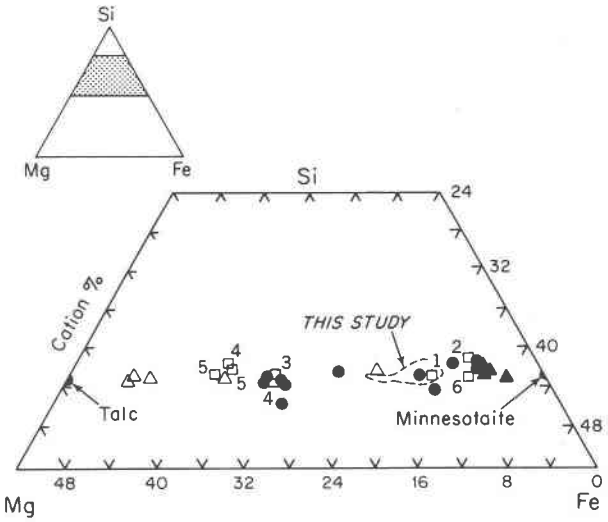

BIWABIK IRON FORMATION
□1 = Gruner (1944)

CUYUNA IRON FORMATION
□2 = Blake (1965)

BROCKMAN IRON FORMATION
□3 = Trendall and Blockley (1970)
□4 = Ayres (1972)
□5 = Miyano (1976)

GUNFLINT IRON FORMATION
● = Floran and Papike (1975, 1978)

SOKOMAN IRON FORMATION
□6 = Zajac (1974)
▲ = Klein (1974)
△ = Lesher (1978)

Fig. 6. Compositional variation of minnesotaite and talc from very-low-metamorphic grade banded iron-formations plotted within the system Fe–Mg–Si.

Textural relations

In the banded iron-formation from D.D.H. 3, interpretation of textural relations allows for the recognition of the earliest mineral assemblages, which are locally well preserved although all show the effect of a low-grade metamorphic overprinting. In some occurrences, however, the early silicates and carbonates have been completely destroyed by reactions. Arrested reaction textures permit possible deduction of these reactions. Textural observations coupled with simplified phase diagrams also permit the deduction of the conditions which the sedimentary or diagenetic mineral assemblages underwent during low-grade metamorphism.

Greenalite generally occurs in magnetite-poor as-

Table 7. Representative electron microprobe analyses of minnesotaite from D.D.H. 3, Weld Range

	1	2	3	4	5	6	7
SiO_2	51.5	51.2	51.3	50.7	50.7	50.9	53.5
TiO_2	0.01	0.02	0.02	0.04	0.04	0.0	0.01
Al_2O_3	0.75	0.83	1.24	1.02	0.85	0.27	0.67
FeO[1]	36.1	35.5	34.5	34.4	33.5	32.6	30.7
MnO	0.35	0.32	0.33	0.40	0.24	0.16	0.21
MgO	5.53	5.73	5.83	6.54	7.00	7.13	10.24
CaO	0.01	0.02	0.00	0.03	0.04	0.04	0.01
Na_2O	0.00	0.06	0.10	0.03	0.08	0.10	0.00
K_2O	0.24	0.24	0.23	0.44	0.27	0.15	0.25
Total	94.49	94.97	93.55	93.60	92.72	91.35	95.65
	Ions on the basis of 11 oxygens						
Si	3.96	3.95	3.95	3.92	3.93	3.98	3.94
Al	0.04	0.05	0.05	0.08	0.07	0.02	0.06
ΣTET	4.00	4.00	4.00	4.00	4.00	4.00	4.00
Al	0.03	0.02	0.06	0.01	0.01	0.01	0.00
Fe	2.32	2.29	2.22	2.22	2.17	2.14	1.89
Mn	0.02	0.02	0.02	0.03	0.02	0.01	0.01
Mg	0.63	0.66	0.69	0.75	0.81	0.83	1.12
Na	0.00	0.01	0.02	0.00	0.01	0.02	0.00
K	0.02	0.02	0.02	0.04	0.03	0.01	0.02
ΣOCT	3.02	3.02	3.03	3.05	3.05	3.02	3.04

[1] *All Fe as FeO*

1. Minn sheaves which cut across intergrowth of qtz-green-stilp. Sample 84715/1; 2. Minn sheaves which radiate into qtz grains in green-sid-qtz assemblage. Sample 84716. 3. Minn sheaves which cut across intergrowth of green-sid-cham-stilp assemblage. Sample 84718; 4. Minn which cuts across ragged stilp aggregate in minn-qtz-rich mesoband. Sample 84734; 5. Minn in green-cham-stilp-sid assemblage. Sample 84719; 6. Minn sheaves cutting sid-qtz grain boundaries. Sample 84737; 7. Minn in Mg-rich sid-cham-py-po mesoband. Sample 84722.

semblages, the most common of which are greenalite–siderite–quartz±pyrite, greenalite–siderite, and greenalite–quartz. Most greenalite-bearing assemblages show an overprinting by stilpnomelane or minnesotaite or both (Figs. 7A and B). Greenalite in these intergrowths is extremely fine-grained (submicron) and appears almost isotropic under crossed nicols. Greenalite aggregates have smooth, 'clean' boundaries with both siderite and quartz. Of the associated sulfides pyrite, very minor pyrrhotite, and arsenopyrite, generally only pyrite is in contact with greenalite, siderite, or quartz, and it occurs as euhedral grains, rarely up to 1.0mm in diameter. Magnetite is uncommon in these mesobands, but where present is euhedral and relatively coarse-grained (0.1–0.8mm), and contains small pyrrhotite inclusions near sulfide aggregates. Grains of all these minerals, with the exception of greenalite, have shapes indicative of minimum interfacial free energy (Vernon, 1976, p. 135–147) and show no evidence of mutual replacement. Greenalite is too fine-grained for grain boundaries to be distinguished, so grain-to-grain relationships cannot be determined. It appears, however, that the greenalite aggregates do not cut across the grain boundaries of other minerals. Such textures seem to indicate that assemblages containing greenalite, siderite, quartz, sulfide, and magnetite are equilibrium assemblages. This conclusion is supported by the consistent distribution pattern of Fe and Mg between coexisting greenalite, siderite, and chamosite (Fig. 4). As no other mineral or mineral assemblage can be directly observed to be a precursor to these minerals, they form the earliest recognizable mineral assemblages in the Weld Range banded iron-formation.

Greenalite also occurs in the Fe-shale bands, where textural relations are generally more equivocal than in the banded iron-formation. Chamosite, greenalite, siderite, pyrite, and minor quartz appear to form the earliest assemblages. No precursor assemblage to these minerals can be recognized and they show no evidence of mutual replacement. Commonly, greenalite and very fine-grained chamosite (<1–$2\mu m$) form separate aggregates that show smooth but irregular contacts. In rare mesobands, greenalite and chamosite are intimately intermixed in fine-grained aggregates.

Greenalite in the early assemblages, both in banded iron-formation and Fe-shale bands, is invariably an Al-bearing variety (Table 2). One mesoband (mesoband 1, sample 84715) contains two distinct greenalite types: an Al-bearing greenalite in the early assemblage of greenalite–siderite–quartz–pyrite, and an Al-poor greenalite which appears to be secondary (Table 2, Figs. 7C and D). The latter, with a grain size similar to the Al-bearing greenalite, is the dominant greenalite type in parts of the mesoband. It is readily distinguished optically by a slightly brown coloring and the presence of variable amounts of dark diffuse patches, similar to those occurring in some Al-bearing greenalites. The contact between the two greenalite types is generally diffuse but may be sharp (Figs. 7C and D). The contact of siderite and quartz with Al-poor greenalite is at high magnification diffuse, with some greenalite occurring within quartz near the contact. Stilpnomelane needles cut across both Al-bearing and Al-poor greenalite (Fig. 7D). Another mesoband (mesoband 2 of sample 84715) contains only Al-poor greenalite in a matrix of siderite, minor quartz, stilpnomelane, pyrite, and very minor magnetite. Stilpnomelane nee-

dles and a mesh of clear greenalite locally cut across or otherwise disrupt siderite–quartz grain boundaries (Fig. 7E).

The secondary Al-poor greenalite in both mesobands appears to have formed at the same time as stilpnomelane. The possible reactions for the formation of these two minerals will be discussed in the section on stilpnomelane. Other Al-poor greenalites in the Weld Range banded iron-formation (Table 2, Fig. 3, and discussed below) also appear to have formed contemporaneously with stilpnomelane, although generally the critical evidence, thought compelling in sample 84715, is lacking.

Chamosite occurs in Fe-shale bands and as a minor constituent in banded iron-formation assemblages. Rocks with significant proportions of both chamosite and greenalite are spatially associated with the Fe-shale bands. In the Fe-shales, chamosite occurs typically as a fine-grained mesh between magnetite and pyrite grains. Generally it is so fine-grained (<1–2μm) that it appears almost isotropic under crossed polars. Slightly coarser-grained chamosite (5–10μm) also occurs as patches and bands in the Fe-shales. Rarely, laths and plates, (20–40μm) of chlorite showing optical properties similar to ripidolite (bluish interference colors masked by green to pale yellow-green pleochroism) occur in the Fe-shales. No difference in composition was found between the chamosite and chlorite by electron microprobe methods.

Siderite is generally fairly coarse-grained (0.3–2.0mm) and shows well-developed grain boundaries (Fig. 7E). Triple junctions among siderite grains and between siderite and quartz grains are common. In greenalite-rich mesobands, siderite commonly forms subrounded aggregates that have sharp contacts with greenalite (Figs. 7A and C). Grain sizes and shapes suggest that siderite has extensively recrystallized. In many assemblages, stilpnomelane and minnesotaite cut across siderite grain boundaries. Rarely, siderite occurs in ragged veins that transgress quartz and appear to be secondary (Fig. 8A).

Quartz occurs mainly in mesobands that contain minnesotaite. It is absent in many greenalite-rich assemblages. Quartz grain sizes (0.1 to 2.0mm) and shapes (triple junctions are common) indicate that it has recrystallized. The presence of quartz veinlets in some assemblages indicates that SiO_2 has been mobile at some stage during diagenesis or low-grade metamorphism.

Magnetite always displays well-developed octahedral faces against coexisting minerals. It does not appear to have taken part in any mineral reactions in these low-grade banded iron-formations because it is never observed in reaction textures. Magnetite grains near aggregates of euhedral pyrite commonly contain small blebs of pyrrhotite. Equilibration between magnetite (or a magnetite precursor) and the original sedimentary sulphide [perhaps mackinawite, $Fe_{1+x}S$ (Berner, 1970)] may have left pyrrhotite grains isolated in magnetite grains during recrystallization.

Sulfides generally display euhedral outlines, except for pyrrhotite inclusions in magnetite. Pyrite generally forms coarse-grained (0.1–1.00mm) aggregates which are concentrated in some mesobands. In some greenalite–pyrite-rich assemblages, trace amounts of pyrrhotite and arsenopyrite occur in contact with the silicates and carbonates. In Fe-shale bands, trains of pyrite grains define a fine lamination. In some minnesotaite-rich mesobands, the assemblage pyrite–pyrrhotite–magnetite–arsenopyrite–siderite occurs in nodules (see below).

Stilpnomelane commonly cuts across contacts between greenalite, siderite and quartz (Figs. 7A, C, D, and E). In mesobands with quartz, stilpnomelane is generally medium-grained (200–350μm, rarely larger), occurring as individual tabular grains or sheaves and rosettes. However, in greenalite–siderite-rich mesobands which lack quartz, stilpnomelane is always fine-grained (50–90μm), occurring as irregular small patches and discontinuous stringers in greenalite (Fig. 7F). In rare, probable intraformational breccias composed of chamosite–greenalite-rich angular fragments cemented by siderite, stilpnomelane grains cut across the fragment–cement boundary and clearly formed later than the breccia.

In some Fe-shale bands, stilpnomelane appears later than chamosite (Fig. 7G) and is concentrated around quartz grains within the fine-grained chamosite matrix. However, in many chamosite–stilpnomelane intergrowths the textures are ambiguous. Rarely, very fine-grained stilpnomelane occurs in monomineralic bands in which there is no evidence of an earlier mineral assemblage.

In rocks composed of coexisting greenalite and chamosite, fine-grained stilpnomelane occurs only within greenalite aggregates, not within slightly coarser-grained chamosite aggregates (Fig. 7H).

Rare textures in two mesobands of sample 84715 appear to provide a key to the stilpnomelane textural relations described above. In mesoband 1 of this sample, Al-bearing greenalite, siderite, and quartz forming the earliest recognizable assemblage are cut across their mutual contacts by relatively coarse laths and sheaves of stilpnomelane. Al-poor greenalite is

present in this mesoband in intergrowths that may or may not contain stilpnomelane. In mesoband 2 of this sample, stilpnomelane and Al-poor greenalite occur in intergrowths in which both minerals cut the grain boundaries of siderite and quartz. The textures in these mesobands are taken to indicate that stilpnomelane and Al-poor greenalite have formed by reaction from Al-bearing greenalite, quartz, and siderite with a K-bearing fluid phase. In many mesobands with Al-bearing greenalite and siderite lacking quartz and secondary greenalite, stilpnomelane occurs in transgressive textures. A stilpnomelane-forming reaction in these mesobands requires that Si, K, and perhaps Al be introduced into the mesoband. It is unclear why secondary greenalite was formed in only some mesobands during the formation of stilpnomelane. It appears that, in mesobands with greenalite and siderite but without quartz (Fig. 7F), the formation of stilpnomelane was hindered by lack of available Si.

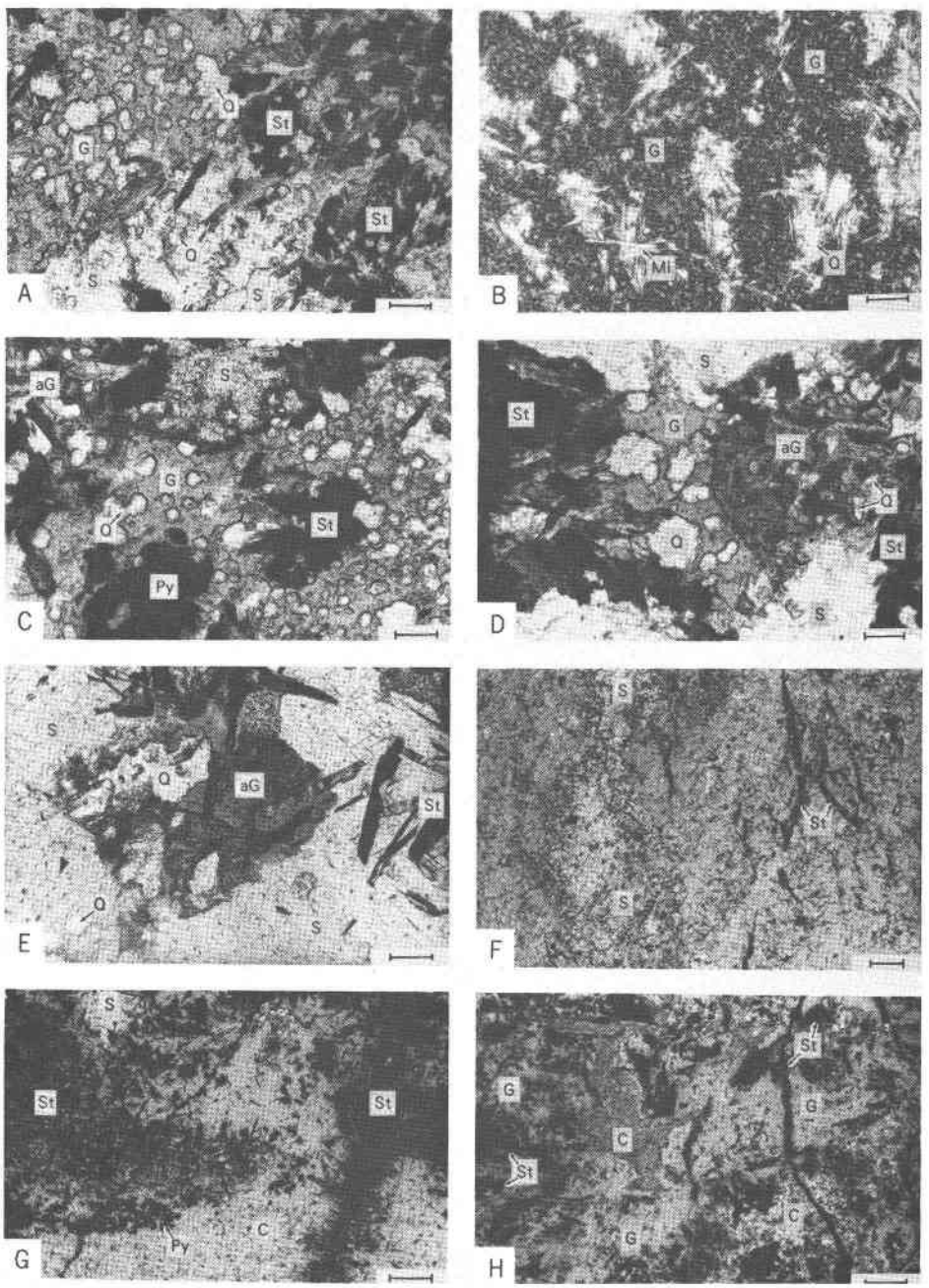

The importance of the availability of Si during stilpnomelane formation is also seen in the Fe-shale bands, which are generally quartz-poor relative to the banded iron-formation. Where stilpnomelane replaces chamosite alone (Fig. 7G), Si and K must have been introduced into the mesoband and Al lost. Where quartz is present in chamosite-rich assemblages, stilpnomelane is relatively coarse-grained and is concentrated around and projects into quartz grains, isolating them from further reaction.

Although the stilpnomelane-forming reactions suggested above indicate considerable mobility of elements during such reactions, the Fe/(Fe+Mg) ratio of stilpnomelane largely reflects the bulk composition of the host mesoband (Fig. 4).

Minnesotaite comprises over 60–70 vol% of many massive mesobands in the Weld Range banded iron-formation, particularly in magnetite-rich parts. These mesobands, which consist of minnesotaite–quartz–magnetite±pyrite, alternate with thick, essentially monomineralic magnetite mesobands. In less magnetite-rich parts, textures indicating partial replacement of quartz–siderite, greenalite–quartz, and greenalite–quartz–siderite assemblages (Figs. 7A and 8A) by minnesotaite are present. Reactions based on electron probe analyses of minerals in quartz–siderite–minnesotaite intergrowths indicate that Mg and Al must have been added as reactants and that Mn and Ca were released into solution. Near one siderite + quartz → minnesotaite reaction site (Fig. 8A), secondary siderite occurs in veins cutting relict quartz. The secondary siderite is slightly enriched in Ca relative to primary siderite (Table 4).

In mesobands containing greenalite–siderite–quartz±sulfides±stilpnomelane, minnesotaite is common in rosettes and sprays of fine needles, cutting across grain boundaries between the silicates and siderite. In greenalite-rich mesobands, minnesotaite occurs as isolated, extremely fine-grained sheaves (5–10μm), whereas on the contact between greenalite-rich and quartz mesobands, massive large sheaves of minnesotaite (200–300μm long) rim and appear to effectively isolate quartz grains from further reaction with greenalite and siderite (Fig. 8A).

In chlorite- and stilpnomelane-rich assemblages, minnesotaite is uncommon except near quartz grains, and even there it forms only a small proportion of the mineral assemblage. In less Al-rich mesobands, stilpnomelane is commonly replaced by minnesotaite (Fig. 8B).

Although minnesotaite is ubiquitous in the banded iron-formation in D.D.H. 3, it generally forms a small proportion (<5–15 vol%) of those mesobands that contain the assemblage greenalite–stilpnomelane–siderite±quartz±pyrite±rare pyrrhotite. Most minnesotaite-rich assemblages (>60–70 vol%) consist of minnesotaite–quartz–magnetite±pyrite.

Minor oxide components in minnesotaite range widely and reflect the compositions of the reactant minerals. For example, minnesotaite formed by the reaction of quartz and siderite has low Al_2O_3 and K_2O contents (*e.g.* anal. 6, Table 7), whereas minne-

Fig. 7. Greenalite, chamosite, and stilpnomelane occurrences at Weld Range.

(A) Extremely fine-grained Al-bearing greenalite (G) and coarse-grained siderite (S) contains subround quartz aggregates (Q). Quartz shows high relief due to minute inclusions. Dark brown, highly pleochroic stilpnomelane (St) cuts across greenalite–siderite–quartz grain boundaries. Sample 84715/1. Scale bar represents 0.1mm.

(B) Crude microbanding defined by alternating laminae of Al-bearing greenalite (G) and quartz–minnesotaite (Q,Mi) assemblages. Greenalite laminae contain small quartz grains. Minnesotaite needles cut laminae boundaries. Sample 84720. Scale bar represents 0.1mm.

(C) Al-bearing greenalite (G), quartz (Q), siderite (S), and pyrite (Py) assemblage. Al-poor greenalite (aG), which contains fine dark inclusions, has diffuse contacts with Al-rich greenalite. Stilpnomelane (St) cuts across contacts between greenalite, quartz, and siderite. Sample 84715/1. Scale bar represents 0.1mm.

(D) Al-bearing greenalite (G) shows sharp contacts with Al-poor greenalite (aG), which contains fine dark inclusions. Siderite (S) and quartz (Q) show sharp, 'clean' boundaries with Al-bearing greenalite but diffuse contacts with Al-poor greenalite. Coarse-grained stilpnomelane sheaves cross-cut greenalite, siderite, and quartz contacts. Sample 84715/1. Scale bar represents 0.1mm.

(E) Siderite (S), quartz (Q), Al-poor greenalite (aG), and stilpnomelane intergrowth (St). Mottled area around greenalite is an extremely fine-grained intergrowth of siderite and greenalite. Minor minnesotaite is present. Sample 84715/2. Scale bar represents 0.1mm.

(F) Fine-grained brown stilpnomelane (St) in stringers in very fine-grained Al–greenalite–siderite (S) mesoband. Fine needles of minnesotaite occur in greenalite. Sample 84716. Scale bar represents 0.2mm.

(G) Stilpnomelane (St) in veins and aggregates in chamosite (C)–siderite (S)–pyrite (Py) assemblage in Fe-shale band. Sample 84734. Scale bar represents 0.1mm.

(H) Fine-grained, dark brown stilpnomelane (St) occurs in greenalite (G) but not chamosite (C) in greenalite–chamosite assemblage in Fe-shale band. Sample 84719. Scale bar represents 0.1mm.

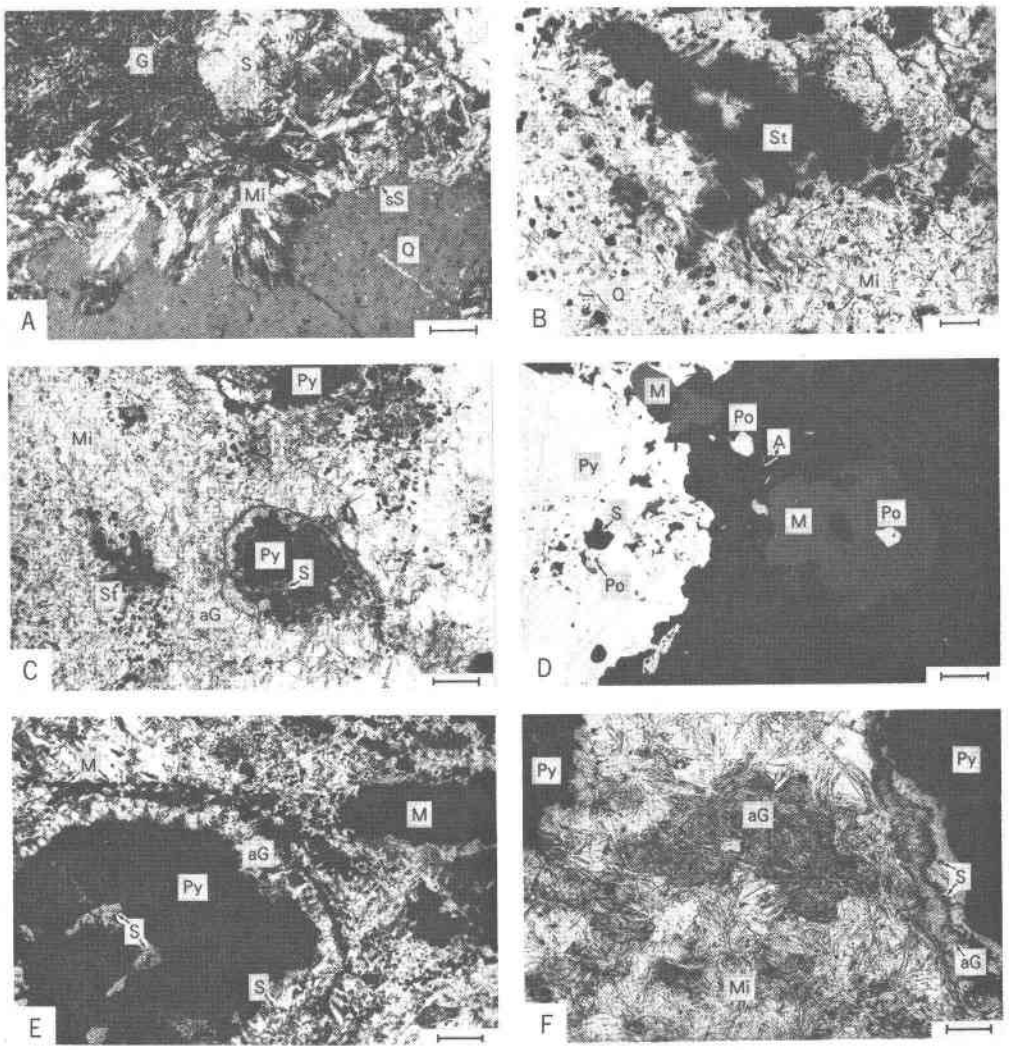

Fig. 8. Minnesotaite textural relations and siderite–sulfide nodules at Weld Range.

(A) Al-bearing greenalite (G), very coarse-grained quartz (Q; grain, not all shown, is 2.5 mm across), and siderite (S) cut by coarse-grained sheaves of minnesotaite (Mi). Minnesotaite forms rim around quartz grain. Extremely fine-grained needles of minnesotaite occur in greenalite away from quartz. Secondary siderite (sS) occurs inside quartz. Crossed polars. Sample 84716. Scale bar represents 0.1mm.

(B) Sheaves and sprays of minnesotaite cross-cutting stilpnomelane. Opaque is magnetite. Sample 84734. Scale bar represents 0.05mm.

(C) Aggregates (Py) of coarse-grained pyrite, minor pyrrhotite, and magnetite surrounded by siderite (S) in nodules rimmed by Al-poor greenalite (aG). Greenalite has sharp contacts with minnesotaite (Mi) and quartz (Q) assemblage. Fine-grained opaque in minnesotaite–quartz assemblage is magnetite. Stilpnomelane (St) is embayed by minnesotaite (see Fig. 8B). Sample 84734. Scale bar represents 0.1mm.

(D) Contact between siderite–sulfide nodule and minnesotaite–quartz±magnetite assemblage shown in reflected light. Nodule consists of an aggregate of coarse-grained pyrite (Py), siderite (S), magnetite (M), and pyrrhotite (Po). Black area consists of siderite (against pyrite aggregate and in contact with large magnetite grain), Al-poor greenalite (rim, 0.03mm wide between siderite and minnesotaite–quartz), and minnesotaite–quartz assemblage (right side of figure). Pyrrhotite and arsenopyrite (A) occur in siderite. Magnetite in minnesotaite–quartz assemblage contains a small pyrrhotite inclusion. Sample 84713. Scale bar represents 0.025mm.

(E) Large siderite (s)–sulfide (Py) nodule with rim of Al-poor greenalite (aG) which shows optical alignment of fibrous grains. Magnetite (M) forms rim between greenalite and minnesotaite–quartz-rich assemblage. Crossed polars. Sample 84713. Scale bar represents 0.1mm.

(F) Ragged and embayed Al-poor greenalite (aG) in minnesotaite (Mi)–quartz (Q)-rich assemblage. Al-poor greenalite in rim of siderite (S)–sulfide (Py) nodule is in contact with minnesotaite and quartz but is not embayed by minnesotaite. Sample 84713. Scale bar represents 0.05mm.

sotaite which replaces stilpnomelane shows relatively high Al_2O_3 and K_2O contents (anal. 1, 3, 4, Table 7). The variable Al_2O_3 (0.27–0.69 wt%) and K_2O (0.07–0.22 wt%) in minnesotaite in one specific mesoband may reflect its formation by a combination of reactions within the mesoband.

Siderite-sulfide nodules are present in several mesobands dominated by the assemblage minnesotaite–quartz–minor magnetite–minor pyrite. Nodules are up to 1.3 mm across and show well defined 60–100μm rims of clear greenalite (Fig. 8C), which occurs in extremely fine-grained fibrous aggregates showing bulk pleochroism from green to pale brown. Greenalite on the outside edge of the vein has sharp 'clean' contacts with minnesotaite, quartz, and magnetite, whereas greenalite (<1–2μm grain size) in minnesotaite–quartz-rich assemblage away from nodules is extensively embayed by minnesotaite (Fig. 8F). Minor stilpnomelane in these mesobands is also embayed by minnesotaite (Fig. 8C). Greenalites, both in nodule rims and in the matrix of the mesoband, have low Al_2O_3 contents, similar to the secondary Al-poor greenalite in sample 84715 (Table 2, Fig. 3).

Greenalite rims do not always completely surround nodules, and in places siderite and pyrite forming the nodules are in contact with quartz or minnesotaite or both. These contacts are sharp and the minerals show no evidence of mutual reaction or replacement. The opaque mineralogy of the nodules consists of pyrite with minor pyrrhotite and magnetite and rarely arsenopyrite (Fig. 8D). Within nodules, pyrrhotite is in contact with pyrite, magnetite, arsenopyrite, and siderite, whereas outside nodules, pyrrhotite occurs only as inclusions in magnetite (Fig. 8D). In one nodule, fine grains of euhedral magnetite are present along the contact between the greenalite rim and the minnesotaite–quartz assemblage (Fig. 8E).

The textures in these mesobands indicate that greenalite in rims of siderite–sulfide nodules is stable relative to greenalite and stilpnomelane in the matrix of the mesoband, and that on the very outside edge of the rim, greenalite is stable in contact with minnesotaite, quartz, and magnetite.

The coexistence of pyrite, siderite, pyrrhotite, and magnetite within the nodules defines the pH and the partial pressures of O_2, S_2, and CO_2. Figure 9 shows the variables f_{O_2}–f_{S_2} at 25° and 325°C. The latter temperature is probably close to the peak metamorphic temperature at the D.D.H. 3 locality (see below). This diagram shows that the assemblage within the nodules defines a lower oxygen fugacity than the coexistence of magnetite–pyrite, which occurs outside the nodules. Also, as siderite does not occur in these mesobands other than in the nodules, the P_{CO_2} in the nodules must have been higher than in the surrounding mineral assemblages. Further, the coexistence of pyrite–pyrrhotite–magnetite defines a higher pH than the coexistence of pyrite–magnetite (Scott, 1974, Fig. S-7). Steep gradients in fluid composition must therefore have existed between the nodules and the host mesoband. That greenalite is stable at lower P_{O_2} relative to the minnesotaite–quartz–magnetite assemblage is shown by the reaction: 4 greenalite + O_2 → 2 minnesotaite + 2 magnetite + 6 H_2O. This reaction is probably responsible for magnetite formation on the outside of the greenalite rim, as seen in Figure 8E. The higher P_{CO_2} within the nodules would also favor the stability of the siderite–greenalite–quartz assemblage over minnesotaite-bearing assemblages. The effect of variations in pH on the stability of

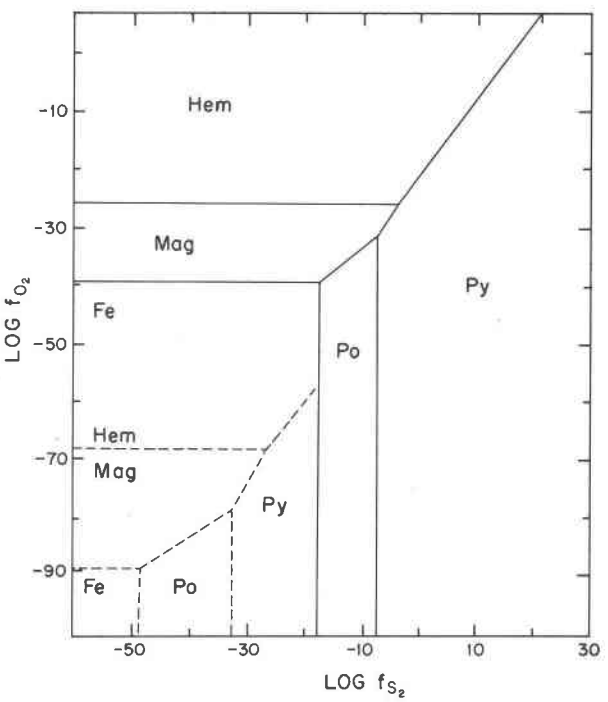

Fig. 9. Stability relations of some iron minerals as a function of f_{O_2}, f_{S_2} and temperature at one atmosphere. Dashed lines are for 25°C and are from Garrels and Christ (1965, p. 159). Solid lines have been calculated from 600°K (327°C) using thermodynamic data from Robie and Waldbaum (1968).

greenalite at temperatures around 320°C is not known, although it may well have an important role, particularly in view of its role in the stability of biotite (Wintsch, in preparation).

Simplified phase relations

Phase relations for greenalite, quartz, siderite, and minnesotaite in the silicate-rich mesobands are shown schematically as a function of temperature and fluid composition (X_{CO_2}) in Figure 10. The fluid is assumed to consist predominantly of H_2O and CO_2 at low temperatures, and at the f_{O_2} assumed for Figure 10 (between the hematite–magnetite and the quartz–fayalite–magnetite buffers) CH_4 will be an important component in C–O–H fluids if graphite is present (Eugster and Shippen, 1967; Ohmoto and Kerrick, 1977). No carbonaceous matter was detected, however, in five samples that were analyzed by the method of French (1964). Further, the presence of a small amount of CH_4 in the fluid will not greatly affect the topology of Figure 10 (Kerrick, 1974). Magnetite is not included in the phase relations, as it generally does not appear to take part in reactions in the low-grade banded iron-formations at Weld Range. In the Gunflint Iron Formation, however, magnetite appears to take part in low-grade reactions, and phase relations involving magnetite with the low-grade minerals are presented by Floran and Papike (1978).

The reactions shown in Figure 10 may also be depicted in isothermal μCO_2–μH_2O diagrams (Burt, 1972; Floran and Papike, 1978). However, a T–X_{CO_2} section is probably more appropriate, because it may be reasonable to assume that both H_2O and CO_2 would not both have been externally-controlled variables (Kerrick, 1974; Greenwood, 1975). If the components in the fluid phase were independent of one another, any assemblage shown in Figure 10 would be as likely as any other to form the 'primary' assemblage in iron-formations. Clearly this is not the case. Textural observations in many iron-formations consistently show that minnesotaite occurs in cross-cutting relationships to earlier mineral assemblages, which almost invariably include greenalite, quartz (or chert), siderite, and other carbonates. This consistency suggests that fluid compositions were controlled by the local mineral assemblages (Greenwood, 1967, 1975; Kerrick, 1974), as is clearly the case in the siderite–sulfide nodules described previously.

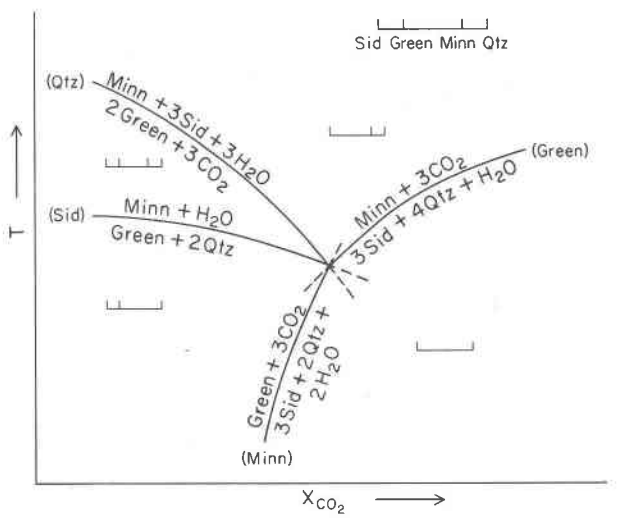

Fig. 10. Schematic T–X_{CO_2} diagram for equilibria in the system FeO–SiO_2–H_2O–CO_2 involving greenalite (GREEN), minnesotaite (MINN), siderite (SID), and quartz (QTZ). Magnetite is stable with all mineral assemblages shown.

The distribution of prograde minerals mapped by Floran and Papike (1975, 1978) in the Gunflint Iron Formation shows that minnesotaite occurs in increasing abundance as the Duluth Intrusive Complex is approached (from Zone 1 to Zone 2 of Floran and Papike, 1978), suggesting that at least some of the minnesotaite-forming reactions are temperature-dependent. If this is so, Figure 10 may be used to explain some of the textural relations seen in relatively simple mesoband assemblages. In bimineralic assemblages of siderite–quartz and greenalite–quartz, fluid composition will not change with increasing temperature until the appropriate minnesotaite-forming reaction is reached. However, fluids coexisting with greenalite–siderite–quartz will be buffered by reactions between these minerals as temperature increases (reaction Minn in Fig. 10). There is no textural evidence to indicate that this buffer reaction, 3 siderite + 2 quartz → greenalite, actually occurred. Textures indicating reaction between siderite, quartz, and greenalite were observed only in sample 84715 and are interpreted as part of the stilpnomelane-forming reaction. Elsewhere, contacts between greenalite, quartz, and siderite are sharp and 'clean.' However, the amount of reaction needed to buffer the fluid composition over the probably small temperature interval from diagenetic conditions to the invariant point from which minnesotaite reactions radiate may not be petrologically evident (see Greenwood, 1975 for full discussion). Once the invariant point is reached by movement along the univariant curve (Minn in Fig. 10), minnesotaite is likely to appear abruptly as a result of the combined opera-

tion of the reactions quartz + siderite → minnesotaite and greenalite + quartz → minnesotaite, with abundant minnesotaite replacing all three earlier minerals. At Weld Range, the mineralogy of silicate-rich mesobands tends to be dominated either by the early assemblages, which are preserved largely because of specific conditions such as low a_{SiO_2}, low P_{O_2}, or high P_{CO_2}, or by the higher-temperature minnesotaite–quartz coexistence. This suggests that reaction of the earlier assemblages to form minnesotaite may have been a rapid process, and is consistent with metamorphic conditions in minnesotaite–quartz-rich mesobands having passed through the invariant point to Figure 10. An alternative explanation, equally consistent with the observations, is that the peak metamorphic temperature was well above those of the minnesotaite-forming reactions, allowing a wide temperature interval for complete breakdown of all reactant minerals in those mesobands where the fluid composition favored minnesotaite-bearing assemblages.

That Figure 10 is applicable only to the higher-temperature side of the greenalite–siderite–quartz stability field is suggested by (a) the presence of minor amounts of minnesotaite in much of the essentially unmetamorphosed Gunflint Iron Formation, well away from the Duluth Intrusive Complex (Floran and Papike, 1975); and (b) the relative stabilities of low-temperature Fe-minerals calculated from thermodynamic data (Klein and Bricker, 1977).

Peak metamorphic temperature

The arsenopyrite geothermometer (Kretschman and Scott, 1976), which correlates the atomic percentage of As in arsenopyrite coexisting with pyrite and pyrrhotite with temperature of formation, indicates a temperature of 320°C for sample 86715 (Table 5). The analytical error in the electron microprobe analysis and the extent of extrapolation from the experimental data points of Kretschman and Scott (1976) suggests this estimate is probably ±50°C.

This temperature is consistent with the metamorphic mineral assemblages in metabasites from near the collar of D.D.H. 3. These contain relict igneous augite and labradorite which are partially replaced by low-Al actinolite, albite, epidote, and chlorite. Available experimental data do not allow an accurate estimation of the minimum temperature for this metamorphic assemblage, although it appears that a temperature of 300±50°C is probable (Zen, 1974; Coombs *et al.*, 1976).

Actinolite in the metabasites becomes progressively more aluminous to the south, across the Weld Range, and in D.D.H. 14 (Fig. 1) moderately aluminous actinolites occur with metamorphic labradorite. These occurrences indicate metamorphic conditions of upper greenschist to lowermost amphibolite facies at low pressure (Liou *et al.*, 1974). There is no direct evidence of metamorphic pressure at the D.D.H. 3 locality, but comparison with other areas suggests it was probably less than 2–3 kbar (Binns *et al.*, 1976).

It should be stressed that 300±50°C is the estimated maximum temperature of metamorphism at Weld Range D.D.H. 3 locality. There is no direct evidence to assess the minimum temperatures of the various reactions in the low-metamorphic-grade banded iron-formations. Minnesotaite can probably form at temperatures as low as 100–150°C. These temperatures are suggested by observations in low-grade Proterozoic iron-formations (French, 1973; Klein, 1974; Klein and Fink, 1976; Floran and Papike, 1975, 1978), by the relative stabilities of the minerals in low-grade iron-formations in theoretical phase diagrams (Klein and Bricker, 1977), and by comparison with the thermal stability of talc (Bricker *et al.*, 1973). Thus at Weld Range minnesotaite probably formed in response to an increase in temperature related to the metamorphic gradient now preserved.

Summary of mineral relations

Based on textural interpretations, the earliest recognizable assemblages in the Weld Range iron-formation include Al-bearing greenalite, siderite, quartz, magnetite, and various sulfide minerals, with chamosite in the more aluminous bulk compositions. Pyrite is the dominant sulfide. Pyrrhotite is rarely part of the assemblage because it generally occurs as inclusions in pyrite or magnetite, and as such is isolated from the remainder of the assemblage. Trace amounts of arsenopyrite and chalcopyrite are also part of the early assemblage. Both the formation of breccia composed of angular fragments and the apparent recrystallization and development of relatively coarse-grained quartz and siderite appear to have occurred prior to the growth of stilpnomelane, which suggests that the banded iron-formation was well lithified before this mineral developed.

Stilpnomelane overprints the early textures and mineral assemblages and is formed by reaction between K-bearing pore solutions and the pre-existing aluminous minerals, Al-bearing greenalite and

chamosite. In some mesobands, a secondary Al-poor greenalite is formed during the stilpnomelane reaction and its growth may have been favored by relatively low P_{O_2}. Reactions based on electron microprobe analysis of reactants and products suggest that there was considerable mobility of components, although the bulk mesoband composition was the dominant influence in determining the Fe/(Fe+Mg) ratio of stilpnomelane. It is clear that the presence of quartz, providing a high a_{SiO_2}, favored stilpnomelane grain growth. In some stilpnomelane-rich mesobands there is no evidence as to earlier mineral assemblages, and it is possible that all earlier textures have been destroyed during recrystallization.

Textures indicate that minnesotaite forms by reaction of greenalite, quartz, siderite, and stilpnomelane. Mesobands composed of minnesotaite–quartz–magnetite±pyrite represent the complete replacement of the precursor assemblages.

Magnetite and pyrite are always euhedral and do not exhibit reaction textures. Both minerals are stable in the earliest assemblages as well as the later minnesotaite-bearing assemblages.

The above mineral assemblages and textural observations for the Archaean banded iron-formation at Weld Range are essentially identical to those described for Proterozoic iron-formations (Klein, 1974; Klein and Fink, 1976; Floran and Papike, 1975, 1978; see French, 1973 for review of earlier studies). This clearly establishes the mineralogical similarities between Archaean and Proterozoic banded-iron formations. Similarities also exist in bulk composition and in sedimentary or diagenetic structures (Gole, in preparation).

The early assemblages are preserved at the peak metamorphic temperature of 320±50°C as estimated for the D.D.H. 3 locality only under certain specific conditions: (a) if the bulk composition was inappropriate for minnesotaite formation, either because of high Al or K contents as in the Fe-shale bands or in Si-deficient assemblages such as in greenalite–siderite mesobands; or (b) if P_{O_2} was relatively low or P_{CO_2} relatively high, or both. The latter conditions would cause greenalite–quartz–siderite assemblages to be stable relative to minnesotaite-bearing assemblages.

Acknowledgments

I thank the Director of the Geological Survey of Western Australia for permission to sample the core from D.D.H. 3, Weld Range. I am also grateful to Cornelis Klein for his support during the latter part of this study and his constructive review of this paper. I thank Mrs. Charles L. Brown for typing. This study was undertaken during tenure of a Commonwealth Postgraduate Research Award at the University of Western Australia. Support from NSF grant EAR-76-11740 (Klein) during preparation of this paper is gratefully acknowledged.

References

Ayres, D. E. (1972) Genesis of iron-bearing minerals in banded iron-formation mesobands in the Dales Gorge Member, Hamersley Group, Western Australia. *Econ. Geol., 67,* 1214–1233.

Ayres, V. L. (1940) Mineral notes from the Michigan iron country. *Am. Mineral., 25,* 432–434.

Bence, A. E. and A. L. Albee (1968) Empirical correction factors for the electron microanalysis of silicates and oxides. *J. Geol., 76,* 382–403.

Berner, R. A. (1970) Sedimentary pyrite formation. *Am. J. Sci., 268,* 1–23.

Binns, R. A., R. J. Gunthorpe and D. I. Groves (1976) Metamorphic patterns and development of greenstone belts in the Eastern Yilgarn Block, Western Australia. In B. F. Windley, Ed., *The Early History of the Earth.* Wiley, London.

Blake, R. L. (1965) Iron phyllosilicates of the Cuyuna district in Minnesota. *Am. Mineral., 50,* 148–169.

Bricker, O. P., H. W. Nesbitt and W. D. Gunter (1973) The stability of talc. *Am. Mineral., 58,* 64–72.

Brown, E. H. (1971) Phase relations of biotite and stilpnomelane in the greenschist facies. *Contrib. Mineral. Petrol., 31,* 275–299.

Burt, D. M. (1972) The system Fe–Si–C–O–H: a model for metamorphosed iron formations. *Carnegie Inst. Wash. Year Book, 71,* 435–443.

Cochrane, G. W. and A. B. Edwards (1960) *The Roper River oolitic ironstone formations.* CSIRO Min. Inv. Tech. Pap. 1.

Colby, J. W. (1971) *Magic IV Program.* Bell Telephone Laboratories Inc., Pennsylvania.

Coombs, D. S., Y. Nakamura and M. Vuagnat (1976) Pumpellyite-actinolite facies schists of the Taveyanne Formation near Loéche, Valais, Switzerland. *J. Petrol., 17,* 440–471.

Eggleton, R. A. (1972) The crystal structure of stilpnomelane: Part II. The full cell. *Mineral. Mag., 38,* 693–711.

——— and B. W. Chappell (1978) The crystal structure of stilpnomelane. Part III. Chemistry and physical properties. *Mineral. Mag., 42,* 361–368.

Eugster, H. P. and G. B. Shippen (1967) Igneous and metamorphic reactions involving gas equilibria. In P. H. Abelson, Ed., *Researches in Geochemistry,* Vol. 2, p. 492–520. Wiley, New York.

Floran, R. J. and J. J. Papike (1975) Petrology of the low-grade rocks of the Gunflint Iron-Formation, Ontario–Minnesota. *Geol. Soc. Am. Bull., 86,* 1169–1190.

——— and ——— (1978) Mineralogy and petrology of the Gunflint Iron Formation, Minnesota–Ontario: correlation of compositional and assemblage variations at low to moderate grade. *J. Petrol., 19,* 215–288.

French, B. M. (1964) Graphitization of organic material in a progressively metamorphosed Precambrian iron formation. *Science, 147,* 917–918.

——— (1973) Mineral assemblages in diagenetic and low grade metamorphic iron-formation. *Econ. Geol., 68,* 1063–1074.

Garrels, R. M. and C. L. Christ (1965) *Solutions, Minerals and Equilibria.* Harper and Row, New York.

Greenwood, H. J. (1967) Mineral equilibria in the system MgO–SiO_2–H_2O–CO_2. In P. H. Abelson, Ed., *Researches in Geochemistry,* Vol. 2, p. 542–547. Wiley, New York.

——— (1975) Buffering of pore fluids by metamorphic reactions. *Am. J. Sci., 275,* 573–593.

Grout, F. F. and G. A. Theil (1924) Notes on stilpnomelane. *Am. Mineral., 9,* 228–229.

Gruner, J. W. (1936) The structure and chemical composition of greenalite. *Am. Mineral., 21,* 449–455.

——— (1944) The composition and structure of minnesotaite, a common iron silicate in iron-formations. *Am. Mineral., 29,* 363–372.

——— (1946) *The Mineralogy and Geology of the Taconites and Iron Ores of the Mesabi Range, Minnesota.* St. Paul Office of the Commissioner of the Iron Range Resources and Rehabilitation.

Guggenheim, S., P. Wilkes and S. W. Bailey (1977) X-ray and electron diffraction study of greenalite and minnesotaite (abstr.). *EOS, 58,* 525.

Jolliffe, F. (1935) A study of greenalite. *Am. Mineral., 20,* 405–425.

Jones, W. R. (1963) The iron ore deposits of the Weld Range, Murchison Goldfield. *Ann. Rep. Geol. Surv. West. Aust., 1962,* 54–60.

Kerrick, D. M. (1974) Review of metamorphic mixed-volatile (H_2O–CO_2) equilibria. *Am. Mineral., 59,* 729–762.

Klein, C., Jr. (1974) Greenalite, stilpnomelane, minnesotaite, crocidolite and carbonates in a very low-grade metamorphic Precambrian iron-formation. *Can. Mineral., 12,* 475–498.

——— and O. P. Bricker (1977) Some aspects of the sedimentary and diagenetic environment of Proterozoic banded iron-formation. *Econ. Geol., 72,* 1457–1470.

——— and R. P. Fink (1976) Petrology of the Sokoman Iron Formation in the Howells River area, at the western edge of the Labrador Trough. *Econ. Geol., 71,* 453–488.

Kretschman, V. and S. D. Scott (1976) Phase relations involving arsenopyrite in the system Fe–As–S and their applications. *Can. Mineral., 14,* 364–386.

LaBerge, G. L. (1966a) Altered pyroclastic rocks in iron-formation in the Hamersley Range, Western Australia. *Econ. Geol., 61,* 147–161.

——— (1966b) Pyroclastic rocks in South African iron-formations. *Econ. Geol., 61,* 572–581.

Lesher, C. M. (1978) Mineralogy and petrology of the Sokoman Iron Formation near Ardua Lake, Quebec. *Can. J. Earth Sci., 15,* 480–500.

Liou, J. G., S. Kuniyoshi and K. Ito (1974) Experimental studies on the phase relations between greenschist and amphibolite in a basaltic system. *Am. J. Sci., 274,* 613–632.

Miyano, T. (1976) Mineral assemblages of the Proterozoic banded iron formation in the Hamersley area, Western Australia. (in Japanese) *Mining Geol., 26,* 273–288.

Ohmoto, H. and D. Kerrick (1977) Devolatilization equilibria in graphitic schists. *Am. J. Sci., 277,* 1013–1044.

Page, N. J. (1968) Chemical differences among the serpentine "polymorphs." *Am. Mineral., 53,* 201–215.

Robie, R. A. and D. R. Waldbaum (1968) Thermodynamic properties of minerals and related substances at 298.15°K (25°C) and one atmosphere (1.013 bars) pressure and at higher temperatures. *U. S. Geol. Surv. Bull. 1259.*

Scott, S. D. (1974) Experimental methods in sulfide synthesis. In P. H. Ribbe, Ed., *Sulfide Mineralogy,* p. S1–S38. Mineral. Soc. Am. Short Course Notes 1.

Trendall, A. F. and J. G. Blockley (1970) The iron formations of the Precambrian Hamersley Group, Western Australia. *Bull. Geol. Surv. West. Aust. 119.*

Vernon, R. H. (1976) *Metamorphic Processes, Reactions and Microstructure Development.* Allen and Unwin, London.

Weaver, C. E. and L. D. Pollard (1973) *The Chemistry of Clay Minerals.* Elsevier, New York.

Whittaker, E. J. W. and F. J. Wicks (1970) Chemical differences among the serpentine "polymorphs": a discussion. *Am. Mineral., 55,* 1025–1047.

Zajac, I. S. (1974) The stratigraphy and mineralogy of the Sokoman Formation in the Knob Lake Area, Quebec and Newfoundland. *Geol. Surv. Can. Bull. 220.*

Zen, E-an (1974) Prehnite- and pumpellyite-bearing mineral assemblages, west side of Appalachian metamorphic belt, Pennsylvania to Newfoundland. *J. Petrol., 15,* 197–242.

Manuscript received, June 13, 1979;
accepted for publication, September 19, 1979.